Fourier Spectrum to Recover Deterministic and Stochastic Behavior in Stirred Tanks

T. Kovács and C. Trägårdh
Div. of Food Engineering, Lund University, 220 00 Lund, Sweden

L. Fuchs
Div. of Fluid Mechanics, Lund University, 221 00 Lund, Sweden

Velocity data from the impeller region of Rushton and 6SRGT pilot-scale impellers were analyzed both in the frequency domain and with respect to periodicity. The four characteristic frequencies and their combination were detected from the Fourier spectrum, and the deterministic part of the signal was recovered by making the amplitude of the other frequencies zero. The deterministic part was then analyzed with tools from nonlinear theories. For the two turbine-types, the dynamics of the deterministic velocity parts were almost identical. The turbulent part of the signal could also be estimated in a similar manner.

Introduction

Usage of rotating impellers is one of the most common ways to perform mixing, and the performance of various radial- and axial-pumping impeller types is studied with numerous methods from mixing time experiments to local flow measurements. For experimental characterization of the flow and turbulence, the main experimental methods used are still laser Doppler velocimetry (Citriniti and George, 2000) and hot-wire anemometry (HWA) (Ståhl Wernersson and Trägårdh, 2000). Using fixed measurement positions in the impeller region, the output signal in both techniques exhibits periodic behavior, the so-called pseudo-turbulence, caused by the passing blades. Since turbulence in this region is neither isotropic nor homogeneous (Rao and Brodkey, 1972), assumptions used to evaluate measured data are not correct (Kresta, 1998). Michelet et al. (1997) presented promising results for handling such turbulence through space–time velocity correlations, and the authors in fact used the periodicity presented in the correlation functions to evaluate the convective velocity.

In order to correct the measured signal, one has to know which periodic component is to be removed. Wu and Patterson (1989) separated the random and periodic fluctuations by reconstructing the deterministic part of the autocorrelation function. In the reconstruction process, they used cosine functions with the frequency of the blade passages (f_b) and twice this frequency. More recent investigations [such as Kemoun et al. 1998)] show that in the power spectrum of a velocity signal, obtained from the centerline of a $D = 0.066$-m Rushton (RT) turbine, many other upper harmonics are also present. These are nonlinearly coupled with some other characteristic frequencies, so that the deterministic part of the measured velocity data corresponds to numerous peaks in the frequency spectrum. In the present article, we use this finding to recover the deterministic velocity component from the measured signal.

Apart from the standard 6RT turbine, we investigated another type, the Scaba Radial Flow Gas Dispersing Turbine with six concave blades (6SRGT). The Rushton turbine has the feature that the power input falls drastically under aeration due to the gas-filled cavities forming behind the blades (Van't Riet and Smith, 1973). Replacing the six flat plates with pipe segments results in a remarkable improvement in the loss of power draw under aeration (Van't Riet et al., 1976), which was utilized in the design of the 6SRGT impeller. This turbine was already studied with respect to power and mixing characteristics [such as Saito et al. (1992) or Galindo and Nienow (1993)].

The purpose of this article is twofold: first, to provide a simple technique for recovering the deterministic component

Correspondence concerning this article should be addressed to T. Kovács.

from the measured velocity data, and second, to analyze this part with respect to the two impeller types presented. The stochastic velocity component is also determined for further comparison.

Pseudoturbulence has no contributions to micromixing, since the frequency content does not enter the energy spectrum of turbulence. By changing the frame of reference to Lagrangian (that is, following a fluid element in the flow), the periodicity would not be noticed (Baldyga and Pohercki, 1995). Thus, extracting the turbulent part of the signal may help in a better description of the mixing properties.

Experimental Setup

The HWA experiments were carried out in a cylindrical stainless-steel tank, $T = 0.8$ m and $H = 1.3$ m, with a flat bottom and four baffles with the width of $T/10$ (Figure 1 and Table 1). The tank was filled with 0.6 m^3 microfiltrated water at a temperature of $T = 16$°C. HWA measurements were made in the discharge of the lower impeller at six fixed radial positions from $2r/T = 0.445$ with 0.02-m interval, referred to as position I, II, …, VI. The rotational speed was set through a Danfoss VLT 5 frequency converter in the range from 80 rpm to 220 rpm, and it was measured with a Lutron DT-2234A digital tachometer.

Table 1. Impeller dimensions

		RT	SRGT
Diameter	D	0.262	0.290
No. of blades	—	6	6
Blade height*	b	0.206	0.155
Blade length*	a	0.267	0.283
Disk diameter*	c	0.680	0.652
Disk-blade edge*	d	0.160	0.174
Blade width*	e	—	0.128

*Normalized with the impeller diameter.

A multiple-channel (DISA CTA 56C01) constant-temperature anemometry (CTA) unit was used with a direction-sensitive split-film probe (Dantec R55 Special). The signals from the DISA CTA 56C17 Wheatston bridges were streamed to a computer through an IOtech Wavebook/512 A/D converter. To achieve high-speed data transfer together with simultaneous sampling, the acquisition system was completed with an enhanced parallel port interface (IOtech, WBK 21) and a Sample&Hold card (IOtech, WBK 11). The CTA system was calibrated for both flow angle and magnitude by placing the probe at the outlet of a free jet. The magnitude calibration was in the range of 0.4–6.5 m/s, while the angle was calibrated from $-90°$ to 90°. To ensure that the measured data series are in the acceptable angle range, the probe was twisted before each measurement until it sensed the main flow direction, which was about 45 degrees at position I. At each measurement, 2^{20} data were collected from both channels simultaneously with the sampling frequency of 7 kHz, which corresponds to a 2.5-min sampling time. The cutoff frequency of the HWA system (in the case of a hot-film probe, it is about 75 kHz) is much higher than the sampling frequency used (Bruun, H. H., 1995). The instantaneous velocities are initially given in the coordinate system of the probe (zero degree means the same detected velocity on both sensor parts). Using the calculated average flow angle relative to the probe, the velocities were transferred to components in the main flow direction (U_1) and to components in the direction perpendicular to it. The Fourier spectrum, calculated with fast Fourier transform (FFT), was used to determine the energy spectrum of U_1 that, upon integration, is related to the time average of velocity fluctuations ($\overline{u_1^2}$) or the variance. Since at the same agitation rate, the power inputs of the two turbine types are very different (Galiando and Nienow, 1993), the to-

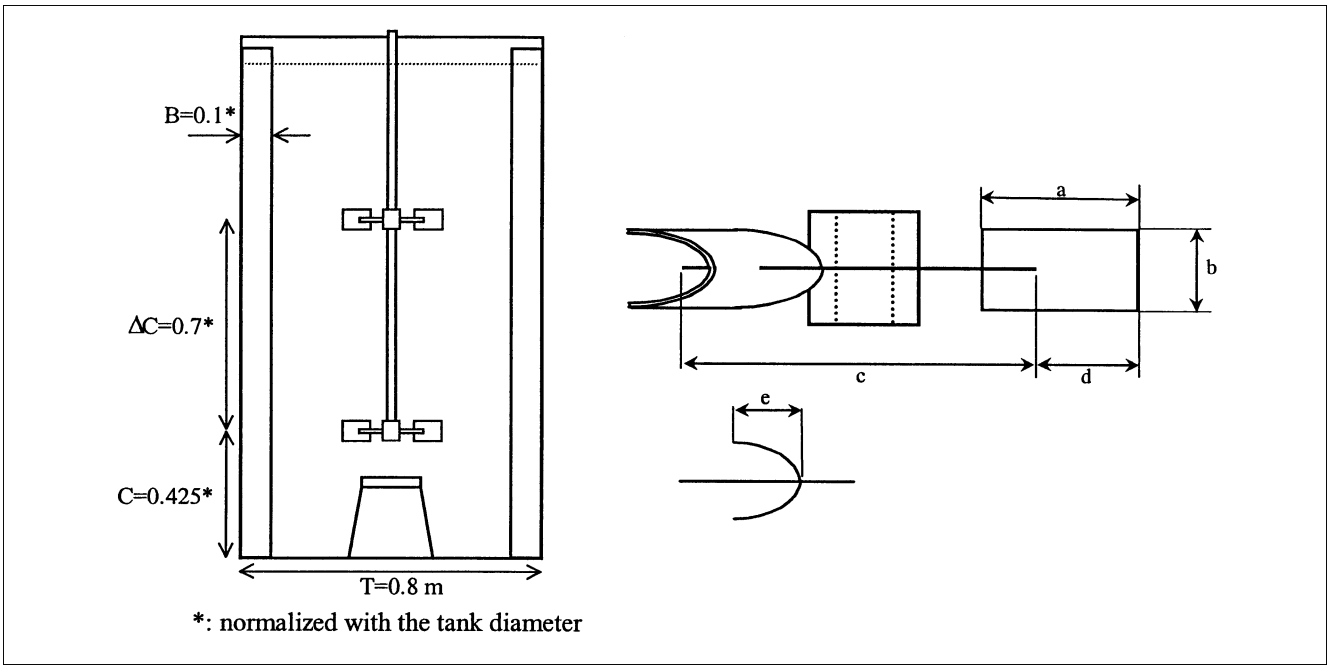

Figure 1. Tank and the 6SRGT impeller.

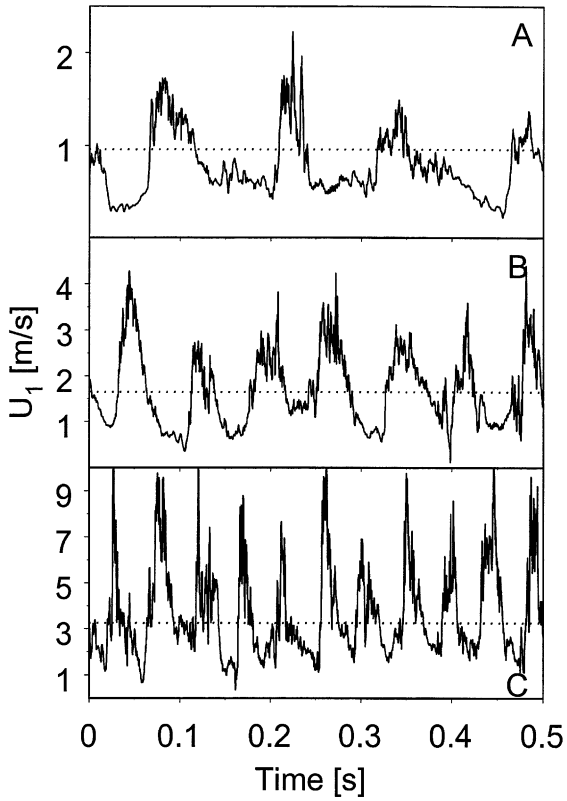

Figure 2. Velocity samples at (a) 80, (b) 140 and (c) 220 rpm, with 6RT at $2r/T = 0.445$; the dotted line shows the mean velocities.

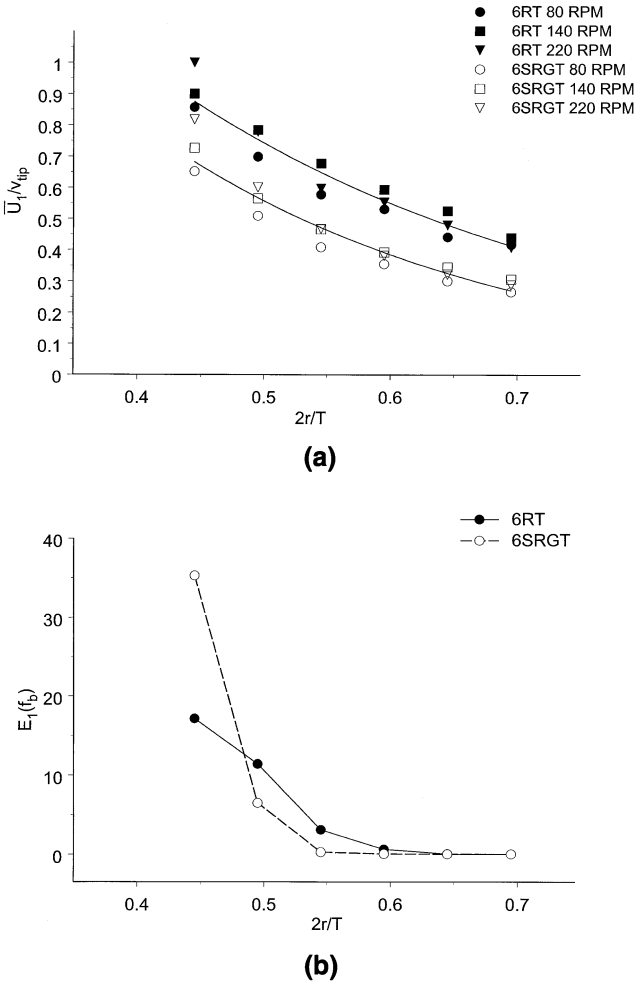

Figure 3. (a) Evaluation of the mean velocity in the center line of the two turbine types; (b) energy of the blade frequency peaks at several radial positions, 140 rpm.

tal power input at each agitation rate has also been measured. The rotating arm of the driving motor, placed on bearings, was connected to a balance, and the total power input was calculated from the torque (M) measurements using $P = ML = 2\pi NmgL$, where m is the output of the balance and L is the length of the arm. With the given impeller geometries, and assuming equal power draw for the two turbines in each configuration, the 6RT consumes about twice as much power as the 6SRGT, and the power numbers ($P_0 = P/\rho N^3 D^5$) were found to be 1.84 for the 6SRGT and 6.0 for the 6RT turbine, respectively.

Results and Discussion

In Figure 2, samples of measured velocities are shown at three different agitator speeds with the Rushton turbine at the closest measurement position to the turbine. The periodicity is clearly recognizable at all agitation rates, with a sudden increase at the beginning of nearly each peak followed by a region with a high level of fluctuations. Note also that the amplitude of the peaks varies rather significantly with time.

Moving toward the wall, the mean velocity decreases according to Figure 3a. As the magnitude of the flow is decreasing, the amplitude of periodicity is also declining, which can be shown by plotting the energy content at the blade frequency from the energy spectra (Figure 3b).

The 6SRGT impeller creates lower velocities at the same agitation rate, but using proper scaling for both the mean velocity and the radial measurement position, the difference between the two turbines presented in Figure 3a can be eliminated. Michelet et al. (1997) have shown that the flow created by a Rushton turbine can be considered as a special kind of plane-free jet, tangential to the disk of the impeller. For the Rushton turbine in our measurement setup, this jet is found tangential to the tip of the impeller blades. In the case of the 6SRGT, the virtual origin of the jet (r_j) is at $r = 0.13$. In Figure 4a, the main velocity data are shown again, but as a function of the distance from the jet origin, normalized with the blade height. When, instead of the tip speed, the velocity at the jet outlet (U_0) is used for normalizing the mean velocity, the big difference between the two curves in Figure 3a vanishes, showing the similar behavior of the main flow induced by the turbines. Using the power input to normalize $\overline{U}_1$, one single curve can again be obtained for both turbines (Figure 4b).

Comparing averaged and normalized values related to the flow and turbulence in the center line of various impeller types may not highlight the differences or similarities. Clearly,

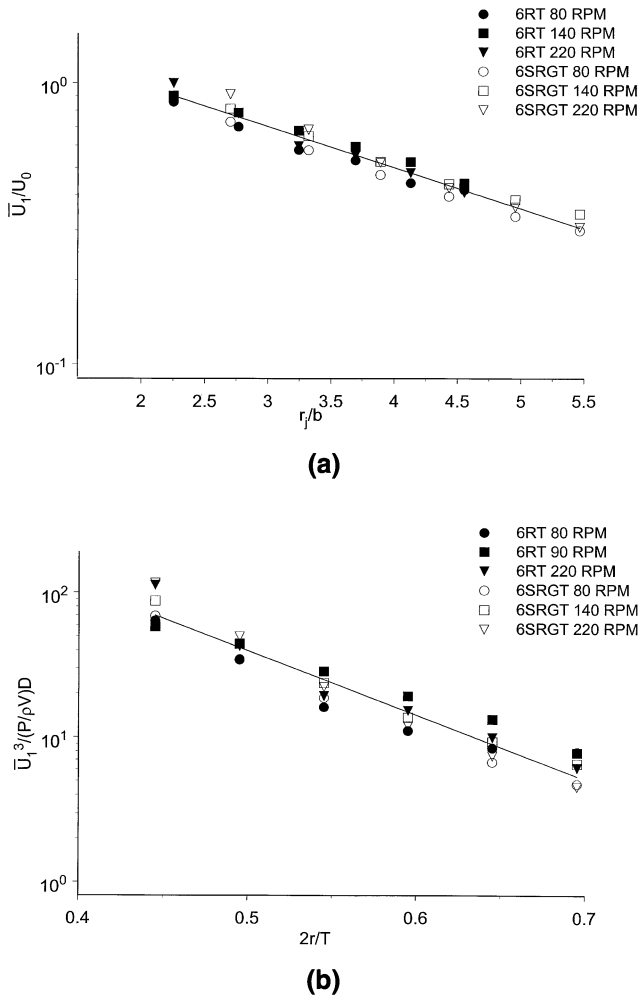

Figure 4. Mean velocity in the center line using (a) the jet representation, and (b) the power input for normalization.

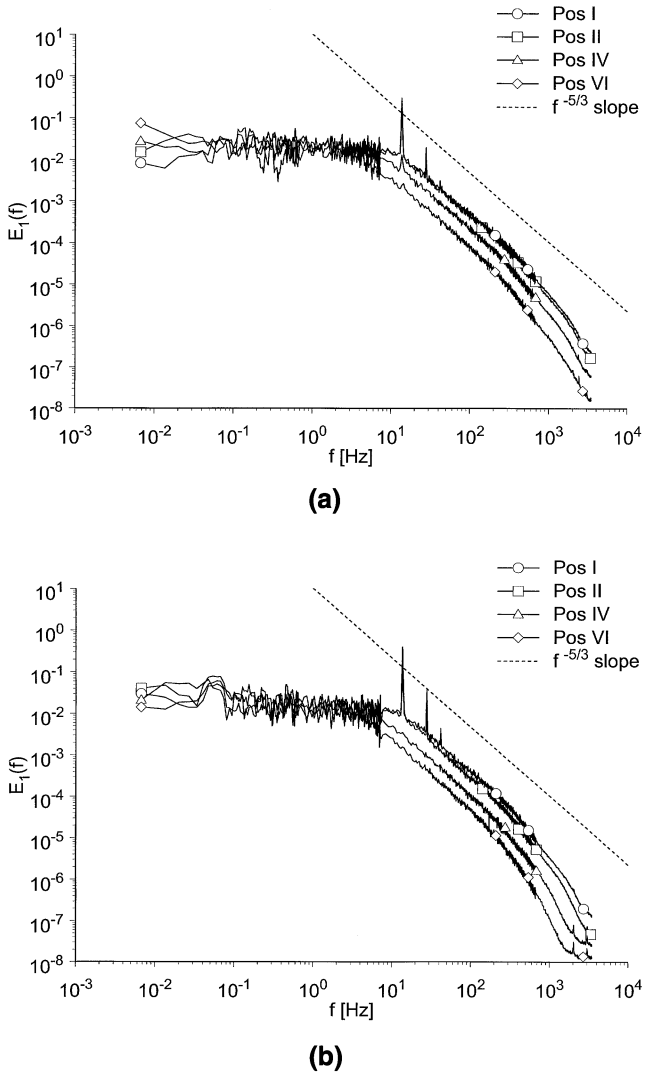

Figure 5. Evaluation of energy spectra in the centerline at 140 rpm for (a) 6RT, and (b) 6SRGT.

one has to try other possibilities, such as changing from time to another domain and analyzing the measured signals in more detail. Comparing the shape of the signals in the frequency domain with the help of the energy spectra at the same agitation rate and various radial positions (Figure 5), one would not notice large differences at first glance. With both turbines at higher frequencies, the energy tends to decrease with the increase of distance from the impeller. At the same time, the slope of the Kolmogorov range does not change. At the low-frequency regions, all spectra have similar values, showing the connection between this region and the apparatus size (Nishikawa and Okamoto, 1976). Note that to overcome the problem of the presenting large data sets, the spectra were smoothed locally, as in Table 2. This method drastically reduces the size of the data to be presented, and at the same time, the inertial subrange becomes better defined (each smoothing range is clearly recognizable).

It was shown earlier that the normalization of the spectra with $\overline{u_1^2}$ (Nishikawa and Okamoto, 1976; Ståhl Wernersson and Trägårdh, 1998) eliminates the large differences due to agitation rate dependence. This result is not surprising, since when the calculation of $\overline{u_1^2}$ (Eq. 1) is considered, this procedure corresponds to area normalization:

$$\sigma_i^2 = \overline{u_i^2} = \int_0^\infty E_i(f)\, df. \tag{1}$$

The result of this operation is shown for the 6RT in Figure 6. From the five agitation rates presented, two groups are formed. The first group contains the lowest two agitation

Table 2. Local Averaging of the Spectra

Frequency Range	Averaging
0.01335–0.66757	Moving average with 5 data
0.67425—7.3433	Average of every 10 data
7.3500–674.915	Average of every 100 data
674.922–	Average of every 1,000 data

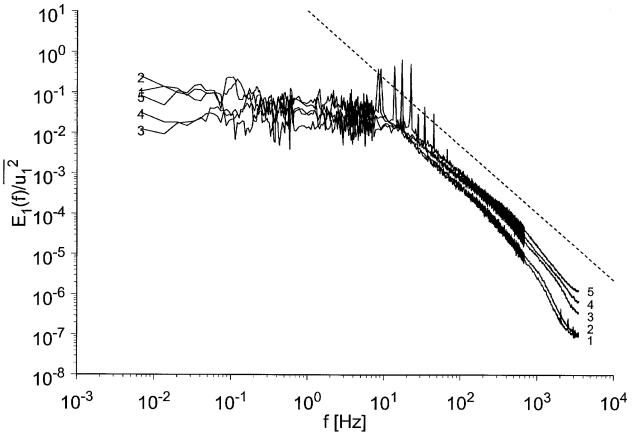

Figure 6. Energy spectra normalized with the $\overline{u^2}$, the numbers from 1 to 5 correspond to 80, 90, 140, 170, and 220 rpm at Position I with 6RT.

rates, while the second has the higher ones. The spectra of 80 and 90 rpm are dominant at the lower frequencies, while in the range of small-scale fluctuations (from about 10 Hz), they are far below the second group. Another difference between the groups is that for the low agitation rates, the slope of the inertial subrange slightly deviates from $f^{-5/3}$. These results together suggest that at 90 rpm, the turbulent Reynolds number is not high enough. Since pseudoturbulence is associated with large-scale fluctuations and in the locally smoothed spectra the differences in agitation rate may fade away, let us focus on the lower frequencies.

Measured signals found in the literature [such as Kemoun et al. (1998)] are typically from vessels with a diameter of about 0.2 m and have a sawtooth pattern, with a low level of local velocity fluctuation and little variation in the amplitude of the peaks (about 6–10% of the average signal height). The energy spectra of such signals are smooth and show harmonics of the blade frequency up to the fifth level, even at relatively low agitation rates (80 rpm).

In Figure 7a, energy spectra are shown up to 50 Hz at 220 rpm, taken at $2r/T = 0.445$ with the 6RT. Despite averaging over four spectra-segments of one measurement (2^{18} data each), the spectrum looks noisy; however, one can still find many sharp peaks. The three characteristic frequencies are the frequency of the blades f_b, the shaft frequency $f_s = f_b/6$, and an unidentified frequency f_q. In addition, upper harmonics and a linear combination of these frequencies are also present. The frequency marked as f_r is related to the periodic horizontal movement of the shaft, which was even observed at the lower impeller during measurements.

Letellier et al. (1997) also detected similar peaks with 88 rpm, at $2r/T = 0.383$ in a vessel with T = 0.2 m and showed that knowing these frequencies, the deterministic part of the velocity signal can be rebuilt using the sum of 44 terms of sine and cosine functions. The new time series can than be qualitatively characterized with techniques used in the characterization of nonlinear dynamics. In our pilot-scale fermenter, energy spectra from velocity data obtained at 80, 90, or 140 rpm at position I only show the blade frequencies and some harmonics. This result shows that even if these frequencies are present close to the blades, they vanish relatively fast (see Figure 3b for comparison).

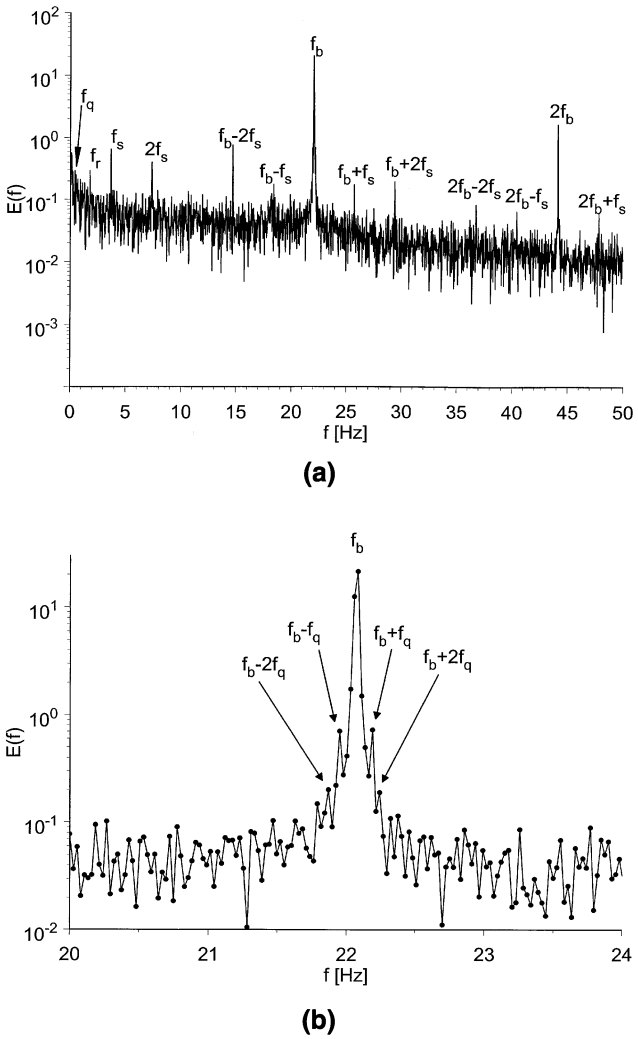

Figure 7. Spectrum at 220 rpm with 6RT, averaged over four spectra each with 2^{18} points, (a) 0-50 Hz and (b) zoom at the blade frequency.

Recovering Deterministic Behavior

Our approach to recovering the deterministic part of the signal originates from the theory of digital signal processing, where most of the operations are done in the frequency domain rather than in the time domain. In general, filtering in the frequency domain is done to keep some desired frequencies and to suppress the rest (Smith, 1997). Passing through the original time series (Figure 8a), a low-pass filter with a 100-Hz cutoff frequency (to keep the third harmonic) does not change the shape of the signal (Figure 8b, solid line). With the sampling frequency and sampling time used, the Fourier spectrum contains about 15,000 data in the 0–100 Hz range of and from Figure 5 it is clear that it corresponds to a large part of the total energy (88.5%) of the signal. Focusing on the blade frequency and its first harmonic only, using a

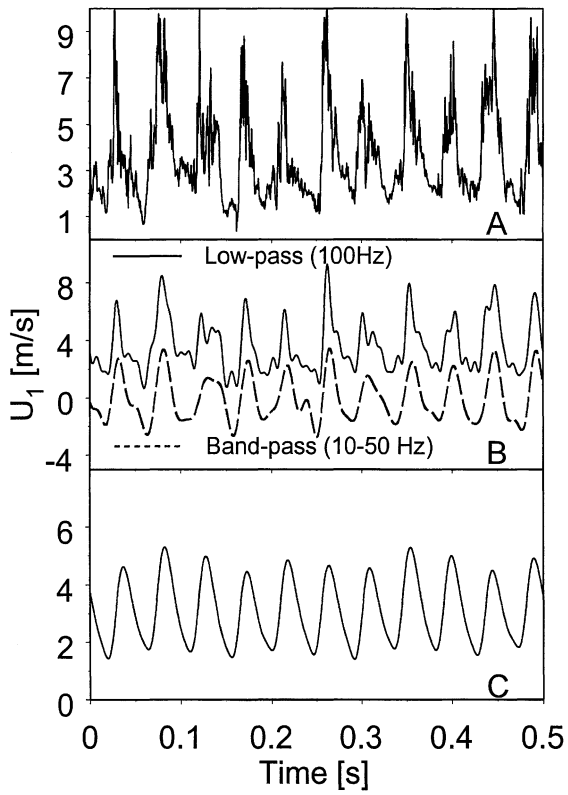

Figure 8. Measured U_1 at 7000 Hz with 6RT at (a) 200 rpm, (b) low-pass and band-pass filtered signal and (c) the reconstructed deterministic part.

band-pass filter in the 10–50-Hz range (Figure 8b dashed line), the shape of the original time series is still recognizable (this range represents 60% of the total energy). Since we cut out the beginning and a large part from the end of the spectrum, the signal tends to be smoother and the differences in the local maxima at each blade passage are drastically reduced. Applying any of these filter types we cannot recover the deterministic part of the signal without including frequencies associated with turbulence.

As was pointed out earlier, frequencies related to the pseudoturbulence are well defined, and browsing through the averaged Fourier spectrum, the exact values of the three fundamental frequencies (f_q, f_s and f_b) and their combinations can be determined (see Table 3). Making all the other frequencies in the spectrum zero (keeping in mind that the Fourier spectrum is symmetrical), and performing an inverse Fourier transform, the deterministic part of the velocity signal can be recovered (Figure 8c).

Although the sampling frequency and time were high enough for proper detection of the frequencies of interest, most of these peaks in the Fourier spectrum do not consist of one single point. In such cases, as in the case of the blade frequency, some of the other neighboring points were also included as frequencies to be kept. The new time series contains only the selected frequencies with the same amplitude as are present in the signal, which makes any further optimization unnecessary and ensures the maximal accuracy allowed by the frequency resolution.

Table 3. 28 Frequencies Associated with Pseudoturbulence, 6RT at 220 rpm

Main Frequencies		Combination with			
Hz	Symbol	f_q	$2f_q$	f_s	$2f_s$
0.134	f_q				
0.268	$2f_q$				
1.30	f_r				
3.68	f_s	±			
7.36	$2f_s$	±			
22.08	f_b	±	±	±	±
44.16	$2f_b$	±		±	±
66.24	$3f_b$	±			

The new signal does not remind us of the original one anymore, and although it only corresponds to the 28 and the additional 56 frequencies in the spectrum, $\overline{u_{1D}^2}$ is still about 40% of $\overline{u_1^2}$.

The probability density function (PDF) of U_{1D} clearly captures its oscillating character (Figure 9) and shows how little information the mean value of such signals holds.

Nonlinear Dynamics

Once the deterministic part, U_{1D}, is extracted, we can analyze its underlying dynamics. The time series of U_{1D} looks like a simple sum of some periodic functions, although some frequencies are nonlinearly coupled, such as

$$\sin(2\pi f_1 t)\sin(2\pi f_2 t) = 0.5\left[\cos(2\pi(f_1 - f_2)t) - \cos(2\pi(f1 + f2)t)\right]. \quad (2)$$

Such time series (or even signals with chaotic oscillations) can be successfully analyzed with the aid of various methods, for example, neural network analysis (Hudson et al., 1990), Hilbert transform (Braun and Feldman, 1997), or vector field reconstruction (Letellier et al., 1995).

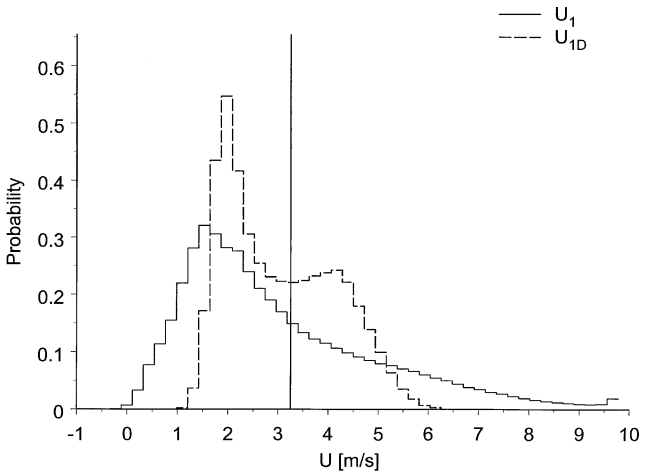

Figure 9. PDF of U_1 and U_{1D} (RT, 220 rpm, Position I), with the mean value marked at 3.25 m/s; to be compared with Figures 2 and 8.

To investigate this nature of U_{1D}, we have performed some nonlinear screening tests analyzed by Ashley and Patterson (2000). The null hypothesis of a linear generating mechanism for this time series can be rejected at the 3.3% level using Tsay and Hinich bicovariance tests and at the 2.6% level using the Brock, Dechert and Scheinkman (BDS) test [all tests were taken from Patterson and Ashley R. (2000)]. In general, the idea behind the tests is as follows: once any linear serial dependence is removed from the data, any remaining serial dependence must be due to a nonlinear generating mechanism. Thus, each of these procedures is actually a test of serial independence applied to the (by construction) serially uncorrelated fitting errors of an autoregression model for the sample data. The next step is to determine the embedding space dimension (d_e). The usual approach is to increase the embedding dimension and then compute the correlation dimensions of the resulting attractors. The computed values keep increasing until the embedding dimension is large enough (Strogatz, 1994). Using the algorithms from Hegger et al. (1997), d_e was estimated to be 4.

To describe the dynamics of the pseudoturbulence the phase space can be generated by either delay or derivative coordinates. For the determination of the optimal time delay (τ), there is no universal method; however, the optimum is around one-tenth to one-half the main orbital period (Strogatz, 1994). For an explicit determination of τ, the first minimum of the average mutual information can be used, which in our case determines the time delay as 8.57 ms. A plane projection of the phase portrait is displayed in Figure 10.

When the noise level of the time series is low, one can also use derivative coordinates for the plane projections. Since the embedding dimension is four, we use four derivative coordinates, namely

$$\begin{cases} X(t) = U_{1D}(t) \\ Y(t) = \dfrac{dU_{1D}(t)}{dt} \\ Z(t) = \dfrac{d^2U_{1D}(t)}{dt^2}. \\ W(t) = \dfrac{d^3U_{1D}(t)}{dt^3}. \end{cases} \tag{3}$$

With these four coordinates, projections can be made onto six planes, which are shown in Figure 11 for the Rushton turbine. Very similar patterns were also presented by Letellier et al., 1997 for the 6RT. The two sets of portraits obtained from the time series of the 6RT and 6SRGT are almost identical to that shown in Figure 12a with an example of the *Y-Z* projection. The figures clearly show how similar the behavior of pseudoturbulence is, close to the turbines at the same agitation rate, without respect to the blade type. Just for comparison, we also made the same projections for the band-pass filtered time series, where although the signal has a low noise level and the periodicity is well pronounced (see Figure 8), the curves obtained do not show clear patterns, as is shown in Figure 12b.

Turbulent Time Series

Having determined U_{1D} by keeping only its characteristic frequencies in the spectrum naturally raises the question: Can we keep the frequencies associated with turbulence instead? The difficulty in this is that due to the finite numerical and time resolutions, a sinusoid-type oscillation does not correspond to one peak in the frequency spectrum, as is illustrated in Figure 13 with an energy spectrum of $\sin[2\pi f_b t]$ (see also Figure 7). In order to eliminate the effect of f_b from the spectrum, one should either remove a reasonably wide frequency range (this would also remove frequencies related to turbulence) or estimate a coefficient with which each frequency around f_b should be suppressed.

Proceeding with the first (more simple) way, about 1,850 frequencies had to be removed from the spectrum to eliminate the effect of the 28 frequencies described. Although these 1,850 frequencies represent only 0.35% of the total 524,288 frequencies, they correspond to 46.3% of $\overline{u_1^2}$ (see Eq. 2). The remaining part is related to the turbulent velocity fluctuations (U_{1T}) and thus, the turbulent kinetic energy. Due to the nature of the generating mechanism, the turbulent time series is intermittent, and since the higher frequencies are kept in the spectrum, most of the short-term structures are similar to the original ones (Figure 14a). The PDF of U_{1T} (Figure 14b) does not show any sign of oscillation or, as a characteristic of the intermittent turbulent signals, the characteristics of the normal distribution.

To show the various levels of periodicity present in the three time series (U_1, U_{1D} and U_{1T}), their autocorrelation is plotted on the same graph in Figure 15. The graph demonstrates how the already strong, original periodicity is enhanced in U_{1D}, but disappeared in U_{1T}, leaving the intermittence as the only sign of its origin. Since the deterministic part corresponds to the large portion of the velocity fluctuations, studying U_{1D} in the case of various turbines may highlight additional properties and differences.

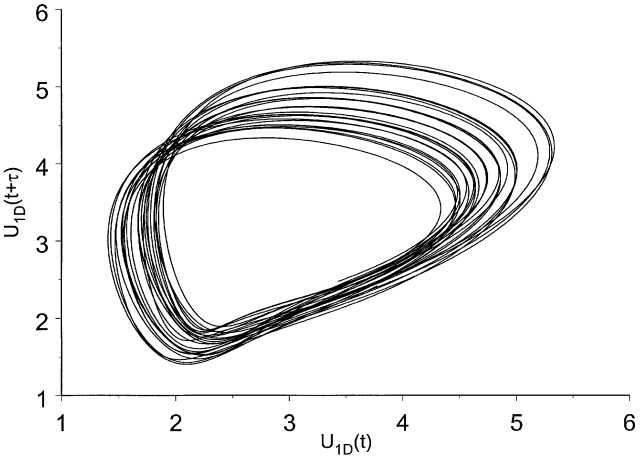

Figure 10. Projection of the phase portrait induced by 6RT at 220 rpm using time-delay coordinates from the reconstructed deterministic part (τ = 8.57 m/s).

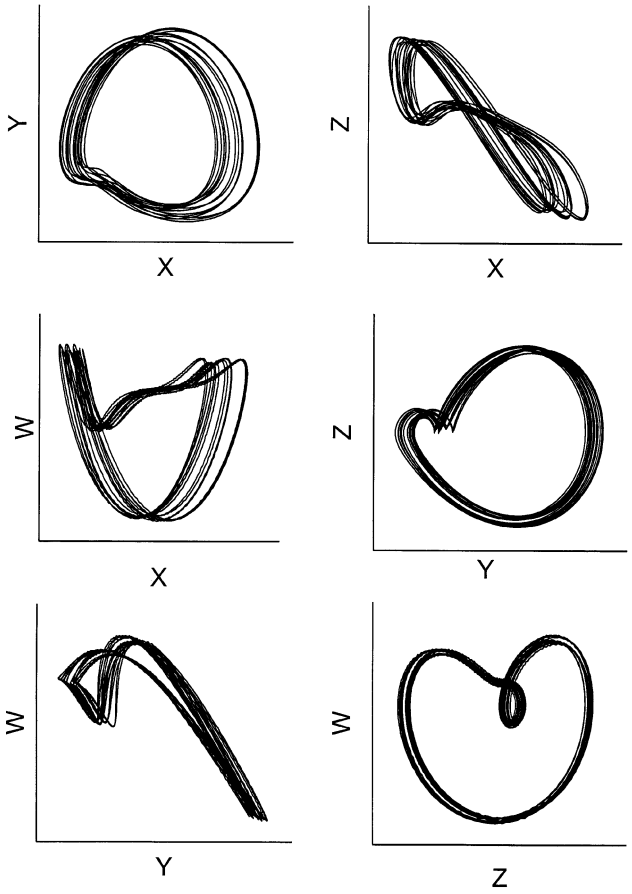

Figure 11. Six plane projections of the phase space from the reconstructed time series using derivative coordinates, 6RT.

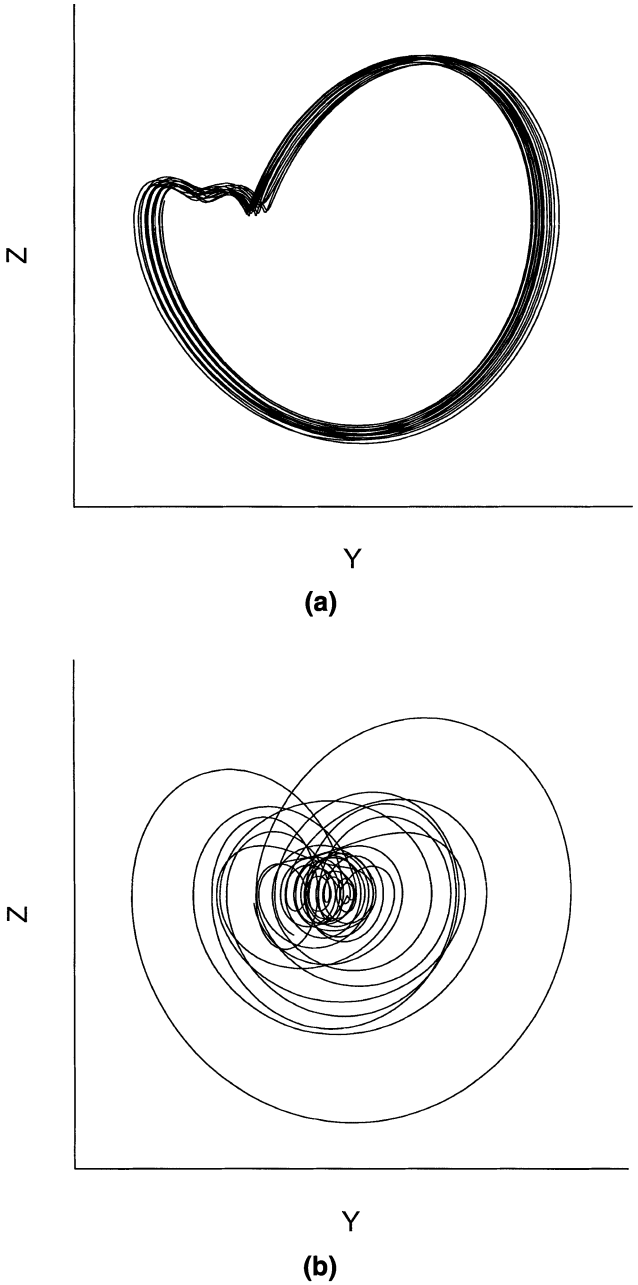

Figure 12. Projections of the phase space to the *Y-Z* plane from the deterministic part with (a) 6SRGT, and (b) the band-pass filtered time series with 6RT.

Conclusions

Instantaneous velocity data were obtained from the impeller region of two types of pilot-scale impellers using constant temperature hot-wire anemometry, with a 7000-Hz sampling frequency and a 150-s sampling time. It was demonstrated that the usual approach of characterizing this type of turbulent time series (that is, present normalized values) may not be sufficient. In moving from the time to the frequency domain, we could see how the agitation rate influences the development of turbulence.

Using the characteristic frequencies and their combinations, which are associated with the periodic movement of the shaft and blades, we could recover the deterministic velocity part. We achieved this by making all the other frequencies zero in the Fourier spectrum. We have investigated time series from the impeller region of 6RT and 6SRGT turbines, and since U_{1D} exhibit strong periodic behavior and their frequencies are nonlinearly coupled, we used methods from the theory of nonlinear dynamics to analyze their behavior. We found the embedding dimension to be four; thus, we could compare the phase portraits using derivative coordinates up to the third level. These phase portraits were found to be almost identical, not surprisingly showing, the same effect of pseudoturbulence on the measured signal close to the blades. Despite the low number of frequencies associated with the pseudoturbulence, they hold about 40% of the original $\overline{u}_1^2$, and so removing the deterministic component has a large effect on the signals' variance. Since the procedure operates at distinct wave numbers or wave-number regions associated mainly with relatively low frequencies, the $f^{5/3}$ slope of the inertial subrange was left unchanged.

The separation method described in the article has a general validity in the study of periodic flow fields, supplying an additional tool for characterization. In the results of compu-

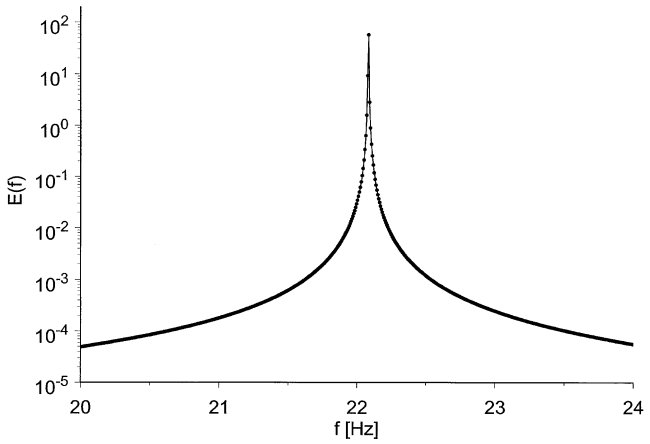

Figure 13. Energy spectrum of $\sin(2\pi f_b t)$, with 2^{20} data and 7 = kHz sampling rate.

tational fluid-dynamics simulations, both the deterministic and stochastic part can be analyzed, which creates the possibility for a more thorough validation.

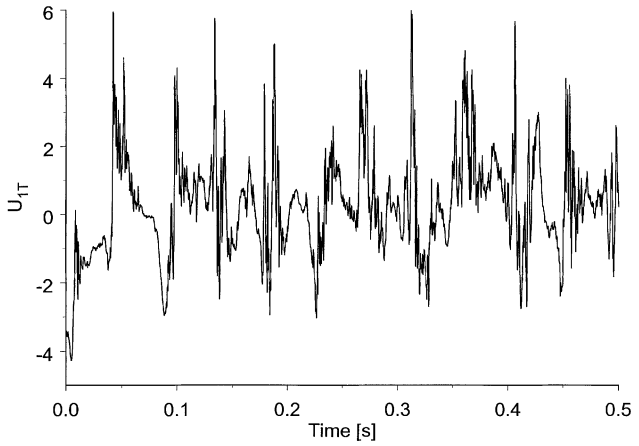

(a)

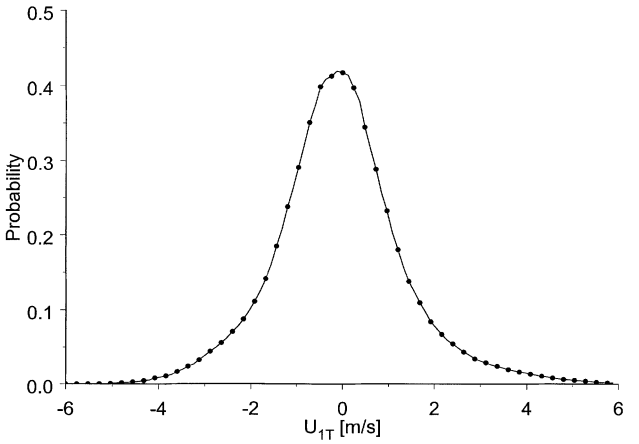

(b)

Figure 14. (a) U_{1T} and (b) its PDF, to be compared with Figure 8.

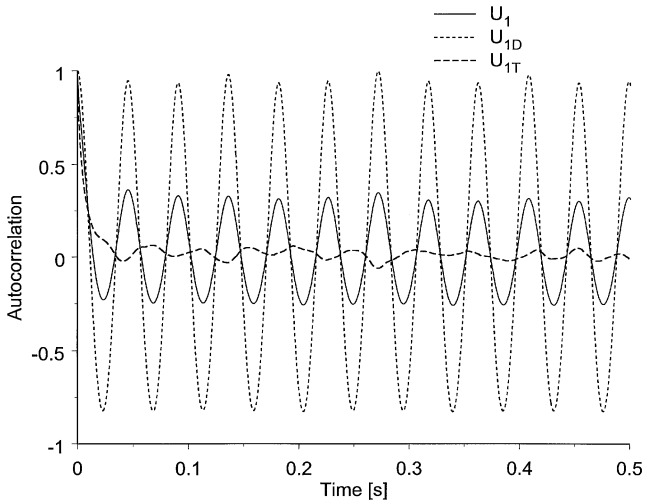

Figure 15. Beginning of the autocorrelation of U_1, U_{1D}, and U_{1T}.

Notation

a = impeller blade length, m
b = impeller blade height, m
c = impeller disk, diameter, m
ΔC = impeller spacing
d = impeller disk blade-edge distance, m
D = impeller diameter, m
e = impeller blade width, m
$E(f)$ = one-dimensional energy spectrum, $m^3 \cdot s^{-2}$
f = frequency, s^{-1}
H = liquid height, m
r = radial tank coordinate, m
R = impeller radius, m
t = time, s
T = tank diameter, m
U_i = velocity, $m \cdot s^{-1}$
u_i = fluctuating velocity, $m^2 \cdot s^{-2}$
$v_{tip} = \pi ND$ = impeller tip speed, $m \cdot s^{-1}$

Greek letters

τ = time delay, s
ρ = density, $kg \cdot m^{-3}$

Subscripts

D = deterministic
T = turbulent/stochastic
1 = indicates properties in the main flow direction

Abbreviations

6RT = Rushton turbine with six flat blades
6SRGT = Scaba radial flow gas dispersing turbine with six concave blades

Literature Cited

Ashley, R., and D. M. Patterson, "Nonlinear Model Specification/Diagnostics: Insight from a Battery of Nonlinearity Tests," Virginia Polytechnic Institute and State Univ. Economics Department, Working Paper E99-05 (2000).

Baldyga, J., and R. Pohercki, "Turbulent Micromixing in Chemical Reactors—A Review," *Chem. Eng. J.*, **58**, 183 (1995).

Braun, S., and M. Feldman, "Time-Frequency Characteristics of Non-Linear Systems," Mech. Systems and Signal Processing, **11**, 611 (1997).

Bruun H. H., *Hot-Wire Anemometry*, *Principles and Signal Analysis*, Oxford Univ. Press, New York (1995).

Citriniti, J. H., and W. K. George, "Reconstruction of Global Velocity Field on the Axisymmetric Mixing Layer Utilizing Proper Orthogonal Decomposition," *J. Fluid Mech.*, **428**, 137 (2000).

Galindo, E., and A. W. Nienow, "Performance of the Scaba 6SRGT Agitator in Mixing of Simulated Xanthan Gum Broths," *Chem. Eng. Technol.*, **16**, 102 (1993).

Hegger, R., H. Kantz and T. Schreiber "Practical Implementation of Nonlinear Time Series Methods: The TISEAN Package," *Chaos*, **9**, 413 (1997).

Hudson, J. L., M. Kube, R. A. Adomaitis, I. G. Keverekidis, A. S. Lapedes, and R. M. Farber "Nonlinear Signal Processing and System Identification: Application to Time Series from Electrochemical Reactions," *Chem. Eng. Sci.*, **45**, 2075 (1990).

Kemoun, A., F. Lusseyran, J. Mallet and M. Mahouast, "Experimental Scanning for Simplifying the Model of a Stirred-Tank Flow," *Exp. Fluids*, **25:** 23 (1998).

Kresta, S., "Turbulence in Stirred Tanks: Anisotropic, Approximate and Applied, *Can. J. Chem. Eng.*, **76**, 563 (1998).

Letellier, C., L. Le Sceller, P. Duterte, G. Gousbet, Z. Fei and J. L. Hudson, Topological Characterization and Global Vector Field Reconstruction of an Experimental Electrochemical System," *J. Phys. Chem.* **99**, 7016 (1995).

Letellier C., L. Le Sceller, G. Gouesbet, F. Lusseyran, A. Kemoun, and B. Izrar, "Recovering Deterministic Behavior from Experimental Time Series in Mixing Reactor," *AIChE J.*, **43** 2194 (1997).

Michelet, S., A. Kemoun, J. Mallet and M. Mahouast, Space-Time Velocity Correlations in the Impeller Stream of a Rushton Turbine, Exp. Fluids, **23**, 418 (1997).

Nishikawa, M. and Y. Okamoto, "Turbulence Energy Spectra in Baffled Mixing Vessels," *J. Chem. Eng. Jpn.*, **9**, (6), 489 (1976).

Patterson, D. M. and R. Ashley, *A Nonlinear Time Series Workshop: a Toolkit for Detecting and Identifying Nonlinear Time Series Dependence*, Norwell, Kluwer (2000).

Rao, M. A. and R. S. Brodkey, "Continuous Flow Stirred Tank Turbulence Parameters in the Impeller Stream," *Chem. Eng. Sci.*, **27** 137 (1972).

Saito, F., A. Nienow, S. Chatwin, and I. P. T., Moore, "Power, Gas Dispersion and Homogenisation Characteristics of Scaba SRGT and Rushton Turbine Impellers," *J. Chem. Eng. Jpn*, **25**, 281 (1992).

Smith, S. W., *The Scientist and Engineer's Guide to Signal Processing*, Chap. 14, California Technical Publishing, San Diego (1997).

Strogatz, S. H., *Nonlinear Dynamics and Chaos*, Chaps. 11 and 12, Addison-Wesley, Reading, MA (1994).

Ståhl Wernersson, E., and C. Trägårdh, Scaling of Turbulence Characteristics in a Turbine-Agitated Tank in Relation to Agitation Rate," *Chem. Eng. J.*, **70**, 37 (1998).

Ståhl Wernersson, E. and C. Trägårdh, "Measurements and Analysis of High-Intensity Turbulent Characteristics in a Turbine-Agitated Tank," *Exp Fluids,* **28**, 532 (2000).

Van't Riet, K and J. M. Smith, "The Behavior of Gas-Liquid Mixtures Near Rushton Turbine Blades," *Chem. Eng. Sci.*, **28**, 1031 (1973).

Van't Riet, K., J. M. Boom, and J. M. Smith, "Power Consumption, Impeller Coalescence and Recirculation in Aerated Vessels," *Trans. Inst. Chem. Eng.,* **54** 124 (1976).

Wu, H., and G. K. Patterson, "Laser-Doppler Measurements of Turbulent-Flow Parameters in a Stirred Mixer," *Chem. Eng. Sci.*, **44** 2207 (1989).

Manuscript received Oct. 5, 2000, and revision received Mar. 3, 2001.